Journal of Zhejiang University-SCIENCE A (Applied Physics & Engineering)

Fractal analysis of small-micro pores and estimation of permeability of loess using mercury intrusion porosimetry

Tuo LU, Yaming TANG, Yongbo TIE, Bo HONG, Wei FENG

Cite this as: Tuo LU, Yaming TANG, Yongbo TIE, Bo HONG, Wei FENG, 2023. Fractal analysis of small-micro pores and estimation of permeability of loess using mercury intrusion porosimetry. *Journal of Zhejiang University-SCIENCE A (Applied Physics & Engineering)*, 24(7):584-595.

https://doi.org/10.1631/jzus.A2200528

The popular six MIP fractal models for pores of porous materials

Few studies based on MIP tests have been carried out on the fractal characteristics of intact Malan loess pores. Questions remain as to whether small-micro pores have a robust fractal feature, and which existing fractal models are suitable for characterizing them

Table 1 The six MIP fractal models considered in the study

Fractal model	Author (year)	Formula expressions
Friesen-Mikula model (Model 1)	Pfeifer and Avnir (1983); Friesen and Mikula (1987)	$log_{10}(\frac{\Delta V_{Hg}}{\Delta P}) = (D_1 - 4)\, log_{10}(P) + C_1$
Neimark model (Model 2)	Neimark (1992)	$log_{10}(A(\leq P)) = (D_2 - 2)\, log_{10}(P) + C_2$
Shen model (Model 3)	Shen, et al. (1995)	$log_{10}(\frac{\Delta V_{Hg}}{d^3}) = -D_3\, log_{10}(d) + C_3$
Zhang-Li model (Model 4)	Zhang and Li (1995)	$\sum_{i=1}^{n} \bar{P}_i \Delta(V_{Hg})_i = C \bullet d_n^2 \left(\frac{(V_{Hg})_n^{1/3}}{d_n}\right)^D$; $W_n = \sum_{i=1}^{n} \bar{P}_i \Delta(V_{Hg})_i / d_n^2$ $\rightarrow log_{10}(W_n) = D_4\, log_{10}(Q_n) + C_4$; $Q_n = \left(\frac{(V_{Hg})_n^{1/3}}{d_n}\right)$
Shen-Li model (Model 5)	Shen, et al. (1995); Li and Horne (2006); Li (2010)	$log_{10}(S_{Hg}) = (D_5 - 2)\, log_{10}(P) + C_5$
Zhang-Weller model (Model 6)	Zhang and Weller (2014)	$log_{10}(\varphi_{Hg}) = (3 - D_6)\, log_{10}(d / d_{max}) + C_6$

Note: $A(\leq P)$: the cumulative fractal surface area smaller than or equal to pressure P, m^2. C or C_m: a constant or the constant produced by the fitting process, where m is 1,2,3…6. D or D_m: the fractal dimension or the fractal dimension calculated by different MIP fractal models, where m is 1,2,3…6. d: pore diameter, m. P: the mercury inlet pressure, Pa. ΔP: the delta between two adjacent P values, Pa. $\bar{P}_i$: the mercury inlet pressure's mean value from P_{i-1} to P_i. S_{Hg}: the mercury saturation (the pockmarks-effect has been eliminated), %. V_{Hg} or $(V_{Hg})_n$: the cumulative volume of mercury (the pockmarks-effect has been eliminated), $m^3\ g^{-1}$. ΔV_{Hg}: the delta between two adjacent V_{Hg} values. φ_{Hg}: the cumulative pore content measured by mercury injection, %.

Role of small-micropores in loess

Types	Macro-meso pores		Small-micro pores	
Concept models (Lei, 1987)	(d≥32 μm)	(32 μm>d≥8 μm)	(8 μm>d≥2 μm)	(2 μm >d)

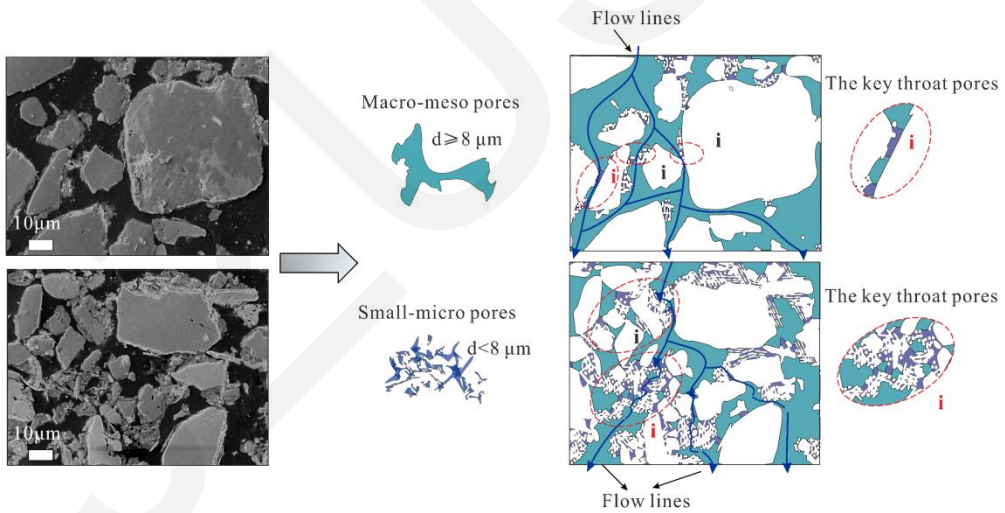

Fig. 1. Role of small-micropores in loess

A significant impact on the throat pores and tunnels for fluid flow.

Box-counting fractal dimension

The box-counting fractal dimension (Li et al., 2009) was taken as a key reference indicator to compare results from the abovementioned six MIP fractal models.

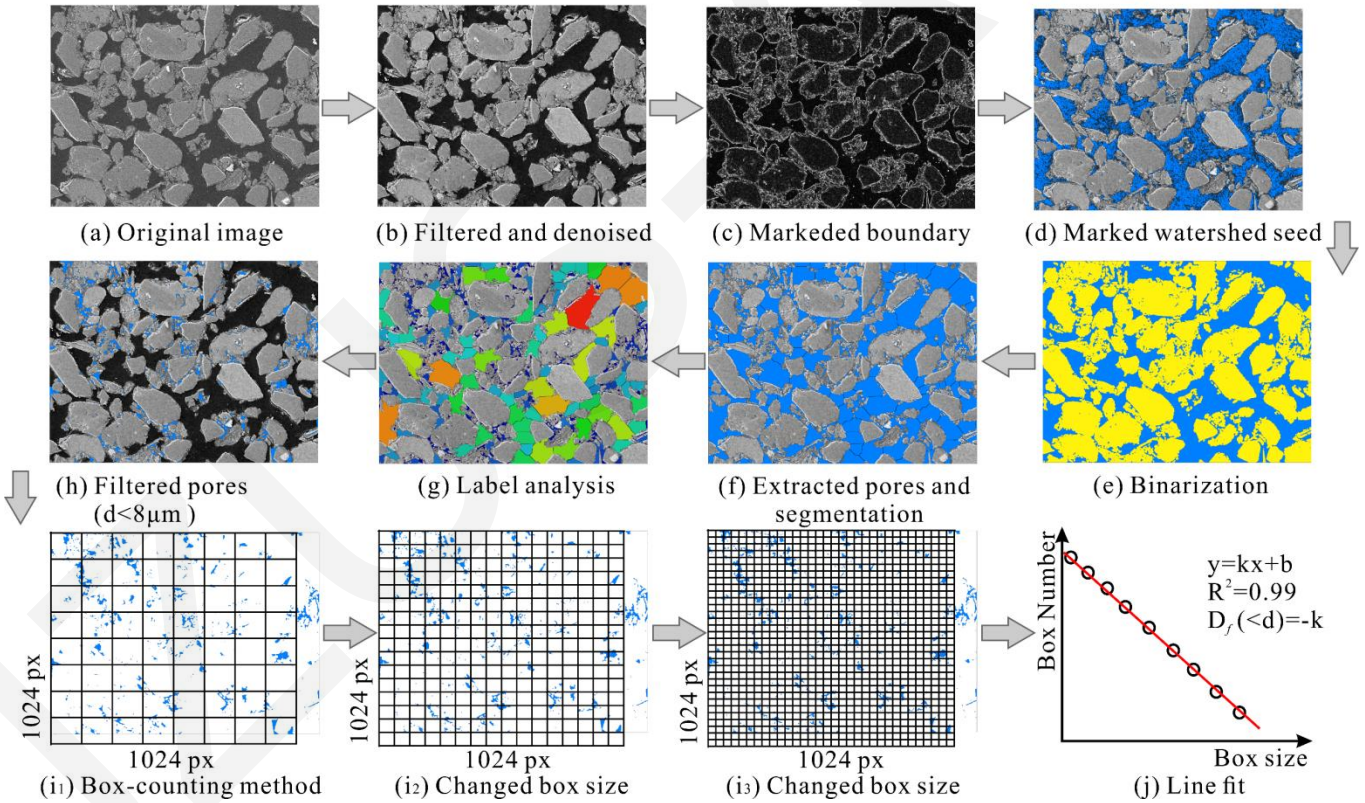

Fig. 2 SEM image processing and the box-counting fractal dimension calculation. (e-f): Blue represents the pores and yellow represents the grains; (g): different colors represent different diameters; (j) linear relationships fitted between the box size and box number

Correlation analysis

Model 2 was suitable for characterising the small-micro pores in this study.

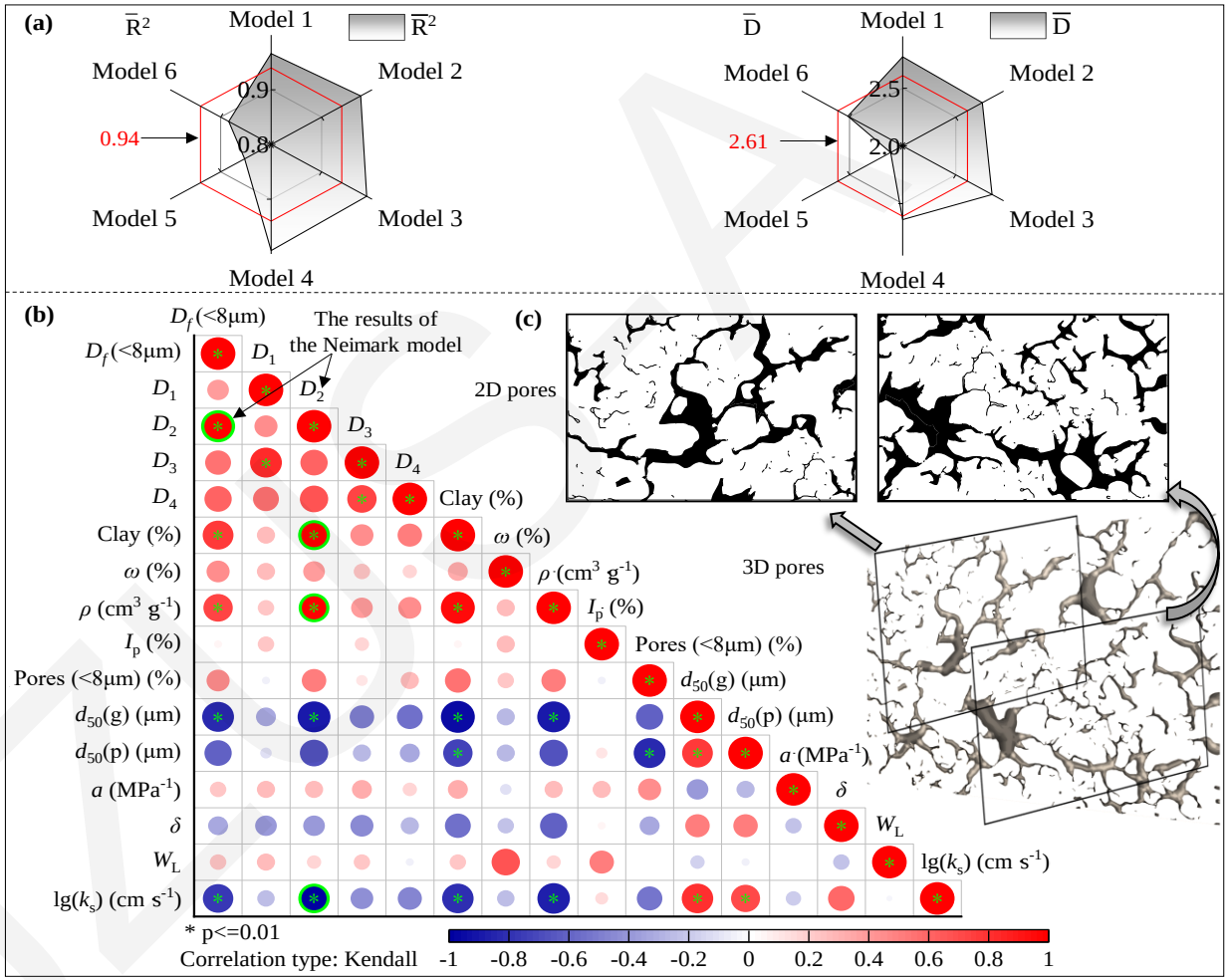

Fig. 3 Correlation analysis. (a) The averages of adjusted R^2 and D values for each model. (b) Correlations between fractal dimensions and physical properties: the green circles represent suitable fractal models and key physical parameters, e.g., saturated water permeability. (c). Relationship between 3D and 2D pore structures

Pore structure characteristics

The pore structure tended to be complex and heterogeneous, with an increasing proportion of small-micro pores. The pore structure also increased the surface roughness. The roughness and heterogeneity led to the 3D-MIP and 2D-SEM fractal dimensions presenting an upward trend. After all, the pore structure, and not the fractal model type, controls the fractal characteristics. Finally, this process decreased the dominant flow line and the water saturated permeability properties.

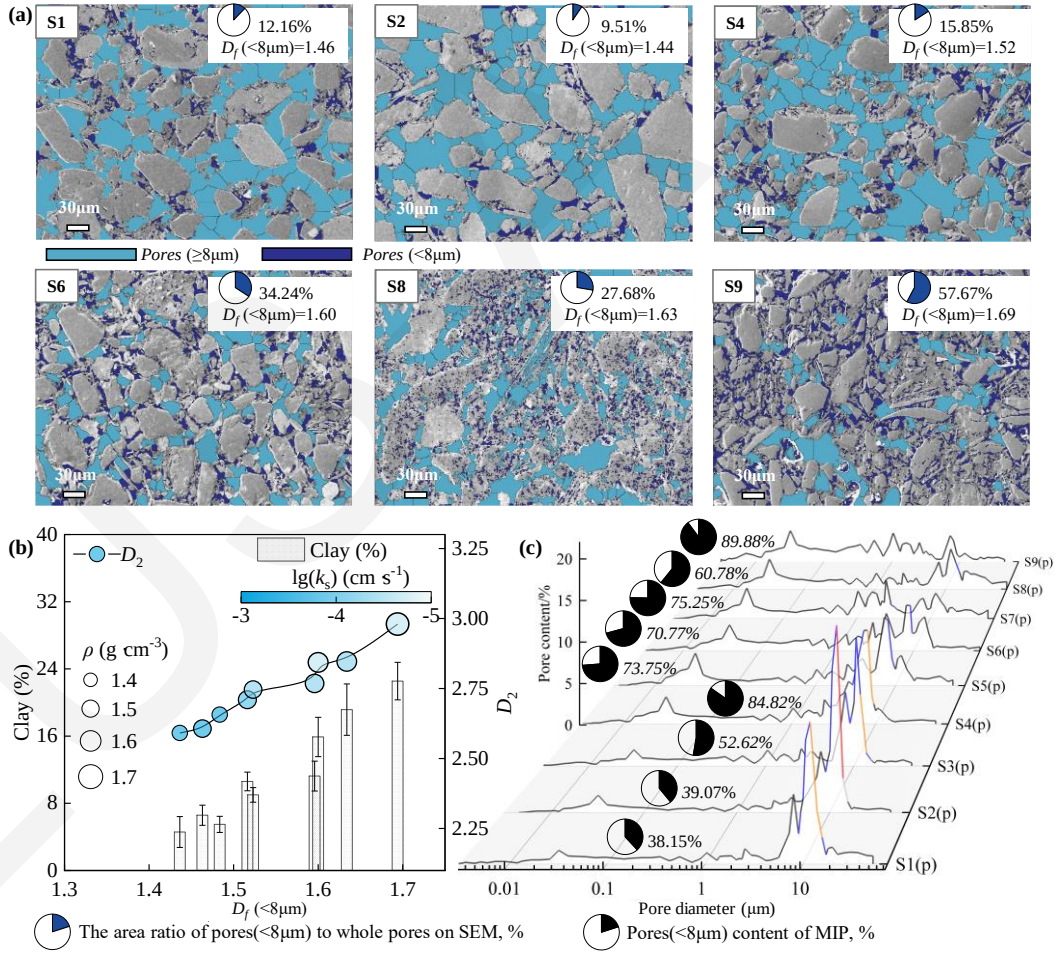

Fig. 4 Pore structure characteristics and results from Model 2 (the Neimark model). (a) Pore structure of the test samples from the SEM test. (b) The fractal dimensions from Model 2. (c) Pore structure of the test samples from the MIP test

Fractal dimensions and evaluation of micro-structure and permeability properties

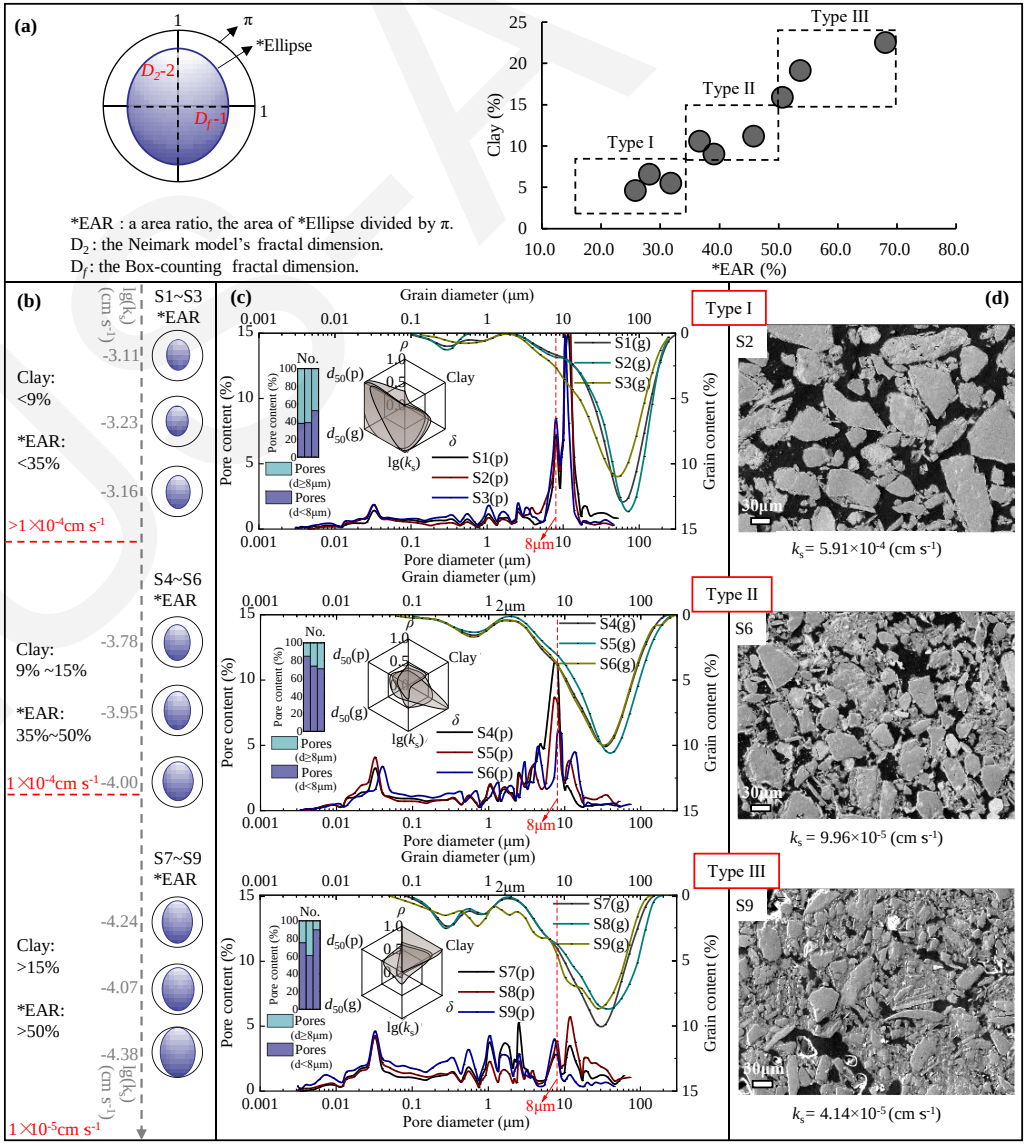

Fig. 4 Fractal dimensions, microstructure, and permeability evaluation. (a) A new specific *Ellipse parameter (*EAR) and microstructure types. (b) *EAR and saturated water permeability. (c) PSD & GSD curves and microstructure types of samples. S(p): pore size distribution (PSD) curves of test samples; S(g): grain size distribution (GSD) curves of test samples. (d) Microstructure observed under SEM

Conclusions

- (1) Model 2 (the Neimark model) of the region of the small-micro pores showed a very good linear fit (decision coefficients greater than 0.94 - the average of all MIP fractal models). The results showed a strong positive correlation with clay content, density, and saturated water permeability, and followed an orderly upward trend that matched that of the box-counting fractal dimensions of SEM images.

- (2) A high content of clay particles leads to an increase in the number of small-micro pores. These small-micro pores also cause more surface roughness and heterogeneity in the pore structure, which tends to present large fractal dimensions. This process leads to a decrease in the content of macro-meso pores and the dominant flow line, thereby degrading the satu-rated water permeability properties.

Conclusions

- (3) A new *Ellipse and its area ratios (*EAR) parameter was introduced in this study, in which the two main half-axes consist of the Neimark model's results (minus two) and the box-counting fractal dimensions (minus one). The *EAR and clay content can be used as valid parameters to quantitatively evaluate the type of loess microstructure and the saturated water permeability. The loess microstructure transitions from type Ⅰ to type Ⅱ when the *EAR is between 35% and 50%, and the clay content is be-tween 9% and 15%. The microstructure further transitions from type Ⅱ to type Ⅲ when the *EAR is greater than 50%, and the clay content is greater than 15%. Correspondingly, the saturated water permeability shows a downward trend in magnitude from 1×10^{-4} to 1×10^{-5} $cm\cdot s^{-1}$. These results can serve as reference values for the classification of the soil microstructure, seepage failure, and water storage of loess in the field of civil engineering.